Since January 2020 Elsevier has created a COVID-19 resource centre with free information in English and Mandarin on the novel coronavirus COVID-19. The COVID-19 resource centre is hosted on Elsevier Connect, the company's public news and information website.

Analytica Chimica Acta 1256 (2023) 341151

Contents lists available at ScienceDirect

Analytica Chimica Acta

journal homepage: www.elsevier.com/locate/aca

Detection of live SARS-CoV-2 virus and its variants by specially designed SERS-active substrates and spectroscopic analyses

Jaya Sitjar [a], Jiunn-Der Liao [a,*], Han Lee [a], Huey-Pin Tsai [b,c], Jen-Ren Wang [b,c], Chien-Hsiung Chen [a], Hao Wang [a], Bernard Haochih Liu [d]

[a] Engineered Materials for Biomedical Applications Laboratory, Department of Materials Science and Engineering, National Cheng Kung University, Tainan, 701, Taiwan
[b] Department of Pathology, National Cheng Kung University Hospital, College of Medicine, National Cheng Kung University, Tainan, 704, Taiwan
[c] Department of Medical Laboratory Science and Biotechnology, College of Medicine, National Cheng Kung University, Tainan, 701, Taiwan
[d] Laboratory for Micro/Nanofabrication and Nanoanalysis, Department of Materials Science and Engineering, National Cheng Kung University, Tainan, 701, Taiwan

HIGHLIGHTS

- SERS-active substrates made to detect live SARS-Co-V-2 virus and its variants.
- Differentiation of variants from peaks attributed to the spike glycoprotein.
- Synergistic hotspot effect to adjacent analytes responsible for virus detection.
- Presence of interfering substance at LOD levels unaffected for reliable detection.

GRAPHICAL ABSTRACT

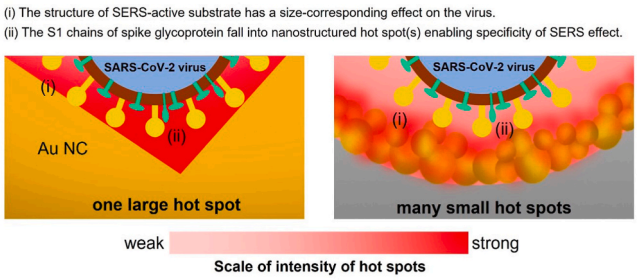

ARTICLE INFO

Handling Editor: Prof. N.W. Barnett

Keywords:
Label-free surface-enhanced Raman spectroscopy
Substrate design
Spike glycoprotein mutated sites
Live SARS-CoV-2 variants
Fast-screening

ABSTRACT

A method using label-free surface enhanced Raman spectroscopy (SERS) based on substrate design is provided for an early detection and differentiation of spike glycoprotein mutation sites in live SARS-CoV-2 variants. Two SERS-active substrates, Au nanocavities (Au NCs) and Au NPs on porous ZrO_2 (Au NPs/pZrO_2), were used to identify specific peaks of A.3, Alpha, and Delta variants at different concentrations and demonstrated the ability to provide their SERS spectra with detection limits of 0.1–1.0% (or 10^{4-5} copies/mL). Variant identification can be achieved by cross-examining reference spectra and analyzing the substrate-analyte relationship between the suitability of the analyte upon the hotspot(s) formed at high concentrations and the effective detection distance at low concentrations. Mutation sites on the S1 chain of the spike glycoprotein for each variant may be related and distinguishable. This method does not require sample preprocessing and therefore allows for fast screening, which is of high value for more comprehensive and specific studies to distinguish upcoming variants.

* Corresponding author. Engineered Materials for Biomedical Applications Laboratory, Department of Materials Science and Engineering, National Cheng Kung University, 1 University Road, Tainan, 70101, Taiwan.
E-mail addresses: jaya.sitjar@gmail.com (J. Sitjar), jdliao@mail.ncku.edu.tw (J.-D. Liao), rick594007@hotmail.com (H. Lee), tsaihp@mail.ncku.edu.tw (H.-P. Tsai), jrwang@mail.ncku.edu.tw (J.-R. Wang), f19980717@gmail.com (C.-H. Chen), eddie115923@gmail.com (H. Wang), hcliu@mail.ncku.edu.tw (B.H. Liu).

https://doi.org/10.1016/j.aca.2023.341151
Received 30 December 2022; Received in revised form 7 March 2023; Accepted 26 March 2023
Available online 30 March 2023

1. Introduction

The emergence of coronavirus disease 2019 (COVID-19) has created an urgent global emergency for those infected, with moderate to severe proportions of high concern, driving the need for accurate and efficient contact tracing, screening, and diagnosis. Vaccination has been shown to slow the rate of increase in cases [1,2]. As of January 2023, at least 64.82% of the global population has received the primary series of vaccines, and 30.55% have received the booster vaccine; as COVID-19 cases have declined, most countries have lifted travel restrictions but emphasized self-management [3,4]. Due to the reported fast transmission of the virus and the rapid emergence of viral mutations, transmissibility and antibody responses may change [5,6]. Despite evidence that some vaccines are effective in preventing the infection of SARS-CoV-2 virus, close monitoring of mutants that develop strong susceptibility to antibody responses is required. As the global pandemic has significantly abated and border restrictions eased as of January 2023, it remains important to research and understand response and mitigation measures taken during the peak of the COVID-19 pandemic to prepare for future outbreaks. Although vaccination has been shown to significantly reduce further transmission, the focus must still be on diagnosis and screening, not only to closely monitor transmission but also to track emerging viral mutations [7,8].

A variety of diagnostic approaches have been utilized to report COVID-19 cases and the most widely used are molecular-based [9,10]. Reverse transcription polymerase chain reaction (RT-PCR), which is of the nucleic acid type, remains the standard diagnostic test for the virus detection. RT-PCR method may yield inaccurate false-negative results, especially in early stages of infection as it relies on amplification of viral genetic material present in a swab sample collected from an individual; an insufficient amount of detectable genetic material may lead to inaccurate results [11]. Although serological tests to detect SARS-CoV-2 antibody in individuals are accurate, they are unsuitable as a detection tool during the early stage of the infection [12]. The point-of-care molecular and antigen detection is simple to operate and can quickly diagnose viruses, but the detection cost is high, and the sensitivity is low, which is still not suitable for simultaneous large-scale rapid screening [13].

Label-free substrate-based surface enhanced Raman spectroscopy (SERS) has demonstrated its potential as a diagnostic tool by providing its characteristic SERS spectra for the detection of various biomolecules, including viruses [14,15]. To achieve signal amplification, the synergistic effect among the nanostructured substrate, Raman laser with a suitable wavelength, and a trace amount of target analyte within the hotspot region is usually considered [16]. To capture an analyte of interest into Raman laser-induced hotspot(s), this can be achieved by matching the size and dimensions of the nanostructure to the analyte, which in this case the relatively large SARS-CoV-2 virus, comprising the structure of spike glycoproteins, is anchored onto the spherical viral particle(s) [17–19].

The SARS-CoV-2 spike glycoprotein is further subdivided into 2 parts - the S1 chain is located at the "head" of the spike, which is more accessible to external environmental particles than the S2 chain, which attaches directly to the spherical virus. The spike glycoprotein is often the site of mutation, especially the receptor-binding domain (RBD) located on the S1 chain [17,22,23]. In this work, several S1 chains are expected to be exposed on the nanostructured substrate, when a Raman laser of appropriate wavelength is applied, thereby forming a hotspot region and containing the S1 chains falling into this region. A method to distinguish variants can be achieved by interpreting the variant-specific SERS peaks of the spike glycoprotein. As the live virus is classified as Risk Group 3 (RG-3), all experiments require testing in a Biosafety Level 3 Laboratory (BSL-3 Lab) [24,25].

2. Materials and method

2.1. Analyte source: live SARS-CoV-2 virus and its variants

Live SARS-CoV-2 viruses are classified as RG-3 organisms [24] and the required propagative work, such as neutralization assays and virus culture should be performed in a BSL-3 Lab [25]. Three live SARS-CoV-2 viruses obtained from the National Cheng Kung University Hospital (Tainan, Taiwan), including GISAID clade lineage A.3 (specimen received at 2020/03/23, GISAID accession ID: EPI_ISL_493203), Alpha (specimen received at 2021/06/09), and Delta (specimen received at 2021/12/10, GISAID accession ID: EPI_ISL_13234976) variants were isolated from the nasopharyngeal or nasal swab samples of infected patients in BSL-3 Lab. The genotypes of these viruses were identified by next generation sequencing (Illumina COVIDSeq Test) or probe-based melting curve assays (VirSNiP Mutation Assays, TIB MOLBIOL, Germany). Respiratory specimens from infected patients confirmed by Roche cobas® SARS-CoV-2 Test were inoculated into Vero E6 cell line containing viral medium (2% fetal bovine serum, minimum essential media and antibiotics). Proliferation was done in a 5% CO_2 incubator at 35 °C, and the cytopathic effect of the cells were monitored by viral growth with an inverted microscope. Virus-infected cells were inactivated by the lysis buffer of RNA extraction kit (QIA amp Viral RNA Kit), analyzed by RT-qPCR in BSL-2 Lab as previously described [26–28], and concentration quantified.

The proliferated virus samples were then subjected to whole gene sequencing to confirm the genotype of the obtained samples in determining SARS-CoV-2 variants. The cultured virus samples were then stored in a freezer at −80 °C in BSL-3 Lab [20]. These variants have essentially the same composition and structure, except for the mutation site expressed on the spike glycoprotein.

2.2. Variant factor: concentration and quality of spike glycoprotein

The samples obtained after proliferation were then set to the highest concentration (100%) and diluted with virus medium to obtain lower concentration samples, i.e. 10^7, 10^6, 10^5, 10^4, 10^3, and 10^2 copies/mL for the study of the limit of detection (LOD). Note that the 100% concentration corresponds to 10^7 copies/mL, where copies are associated with the nucleic acid signature of a variant; however, viral particles may be alive or dead (e.g., denatured, inactivated or fragmented matter). To determine the LOD, 10^7 copies/mL original virus concentration was used as the reference.

There were differences in the quality of spike glycoproteins under different treatment conditions. For example, when the spike glycoprotein is isolated or inactivated from a live SARS-CoV-2 virus, a different spike glycoprotein from that in the live virus may be produced. In our previous study [20], a live S pseudovirus was synthesized using the spike glycoprotein from the hCoV-19/Wuhan/WH01/2019 virus [28], and its characteristic SERS spectrum was used to correlate with that of live A.3 variant in this study. Although these two spike glycoproteins are mostly similar in chemical composition and structure, the Raman peak assignment of spike glycoproteins in the literature remains a challenge to the original quality.

2.3. SERS-active substrates

In Fig. 1 (i) and (ii), surface morphologies of substrates are shown. The substrates used in this study are Au nanocavities (Au NC) and Au nanoparticles on porous ZrO_2 (Au NPs/pZrO_2). Au NCs were fabricated through a nano-indenter wherein the indentation depth is 120 nm, and the tip-to-tip displacement is 600 nm. Au NPs/pZrO_2 were fabricated through the deposition of Au NPs on a porous ZrO_2 platform; this porous ZrO_2 was made through annealing ZrO_2 gel-like precursor spin-coated on Si wherein polystyrene nanoparticles (PS NPs) with a diameter of 250 nm were deposited, and the annealing process simultaneously

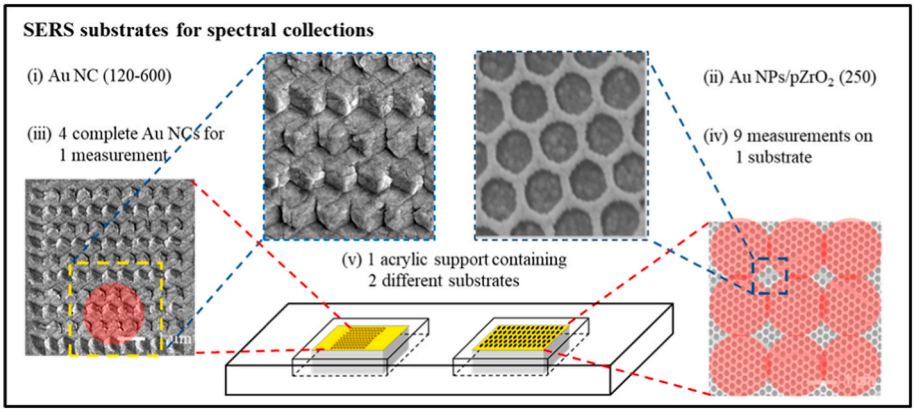

Fig. 1. The SERS-active substrates utilized in this study are Au NC (i) and Au NPs/$pZrO_2$ (ii), each having ~4 (iii) and 36 nanostructures within 1 Raman spot, respectively. SERS measurements were done in nine adjacent spots (iv) that correspond to more than 36 and 324 measured nanostructures; substrates were placed on acrylic support throughout the collection of SERS signals (v).

formed the ZrO_2 and removed the PS NPs, leaving behind a porous substrate. Both substrates were shown to be effective SERS substrates for the detection of live S pseudovirus [20] and will be used in this study to explore SERS spectra of live viruses and to develop a method to differentiate the variants by spectroscopic analysis. Au NCs have a diagonally arranged cavity-like structure in which each cavity has a large hotspot. Au NPs/$pZrO_2$ have concave bowl-like structures arranged in a hexagonal array with multiple small hotspots on each bowl, which is due to the Au NP clusters covering the substrate surface. Within a Raman laser spot of the portable Raman Spectroscope (portable RS), there are ~4 and ~36 complete nanostructures, which are referred to as the entirety of a unit of nanostructure, included for Au NCs and Au NPs/$pZrO_2$, respectively.

2.4. Instrument resolution and consecutive measurements

All the experiments to detect live SARS-CoV-2 virus and its variants were performed in the BSL-3 Lab using a portable Raman Spectroscope (denoted as portable RS, Benchtop-size Single Laser Micro Raman Spectroscopy, NS220, Nanoscope Systems, Inc., Korea) with a laser spot size of ~2 μm in diameter, a spectral resolution of ±10 cm^{-1}, and a laser wavelength of 633 ± 1 nm. For comparison, the data for live SARS-CoV-2 S pseudovirus were obtained using a laboratory Raman Spectroscopy (denoted as lab RS, UniDRON, CL Technology Co. Ltd. Taiwan) with a laser spot size of ~1 μm in diameter, a spectral resolution of ±5 cm^{-1}, and a laser wavelength of 633 nm with a laser power of 35 mW; the experiments were performed in the BSL-2 Lab. The Raman laser intensity produced by portable RS is expected to be relatively weaker than that produced by lab RS, due to the limited capability making it less sensitive.

In Fig. 1 (iii) and (iv), an experiment contains nine consecutive measurements of ordered nanostructures (i) and (ii) and with a center-to-center distance of ~2 μm (iii). The test sample is first placed 10 μL of the analyte-containing solution in a shallow well on a plastic slide with a glass coverslip containing a 5 mm × 5 mm support and two substrates.

2.5. Spectral data acquisition and processing

The raw spectral data were processed for background subtraction using OriginPro software. SERS spectra were acquired from nine adjacent positions for all six concentrations of analytes and all three variants. To compare SERS spectra of S pseudovirus (Fig. 2) with variants (Fig. 3) and substrates (Fig. 4), the average spectrum for each variant was taken from nine positions per substrate at a concentration of 10^6 copies/mL were used. To interpret why the average is taken, it is important to note that the band shift of the portable spectrometer shows slightly wider than that of the laboratory one. In Supporting data (SD 1), to verify the difference between nine measurements, in comparison with three fixed peaks offset (SD 1a), regions are programmed to be ±5 cm^{-1} from the fixed peaks within which the maximum point of the characteristic peaks can be found (SD 1b). With the latter approach, the peak shifts resulting from the portable spectrometer resolution are taken into consideration; the variance among the intensities of each characteristic peak from the nine spectra were also analyzed.

More of the same measurements can be made owing to the wide range of ordered and repetitive nanostructures on the substrate. The spectral range from 600 to 1800 cm^{-1} was chosen as this range includes most of the characteristic peaks of the virus. To determine the LOD for each substrate and three variants, specific peaks, especially those for the qualitative detection of live SARS-Co-V-2 virus, were chosen and labeled on the obtained spectra; analyte concentrations of 10^7, 10^6, 10^5, 10^4, 10^3, and 10^2 copies/mL were measured. For the estimated LOD, at least one measurement location should have an observable SERS spectrum after nine consecutive measurements. To distinguish variants, different SERS substrates and variants were cross-examined. The specific peaks of the variants as well as peak shape changes in the spectra were investigated.

3. Results

3.1. Comparison of SERS spectra of live A.3 variant and S pseudovirus

In Fig. 2(a), the structure and composition of the surface proteins of a general live SARS-CoV-2 virus and SARS-CoV-2 S pseudovirus (referred to as S pseudovirus) are depicted, respectively. They differ by the membrane glycoprotein (a-1) and envelope glycoprotein (a-2) of live virus and the lentiviral packaging vector (a-4) of S pseudovirus. The spike glycoproteins associated with live virus and S pseudovirus are denoted as (a-3 L) and (a-3 P), respectively.

In Fig. 2(b) and (c), SERS spectra of previously identified S pseudoviruses using (i) Au NC and (i') Au NPs/$pZrO_2$ as substrates were used as references [20] The spike glycoprotein (a-3 P) of S pseudovirus was synthesized by that of hCoV-19/Wuhan/WH01/2019 virus [29], and its characteristic SERS spectra were first compared with the spike glycoprotein (a-3 L) of GISAID clade lineage A.3 variant (referred to as A.3 variant), which has two unique surface proteins (a-1) and (a-2) and are absent in the pseudovirus form, but lacks the surface protein (a-4). Therefore, SERS peaks corresponding to (a-3 P) and (a-4) can be used as references to distinguish those corresponding to (a-1), (a-2), and (a-3 L) from A.3 variant. Spectral analysis compares SERS spectra by their common and unique proteins. Major corresponding SERS characteristic

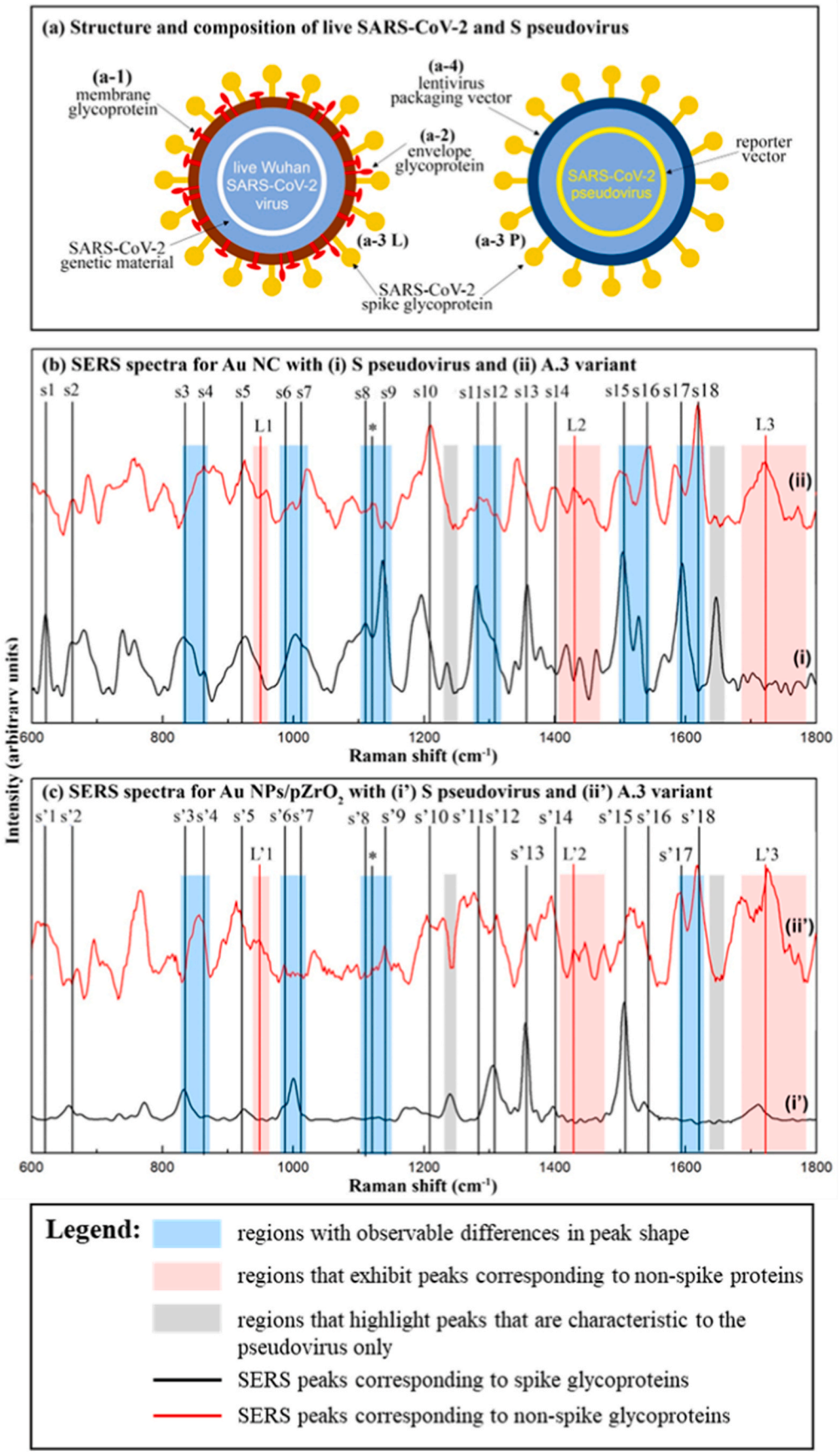

Fig. 2. (a) Structure and composition of S pseudovirus and A.3 variant; components are labeled: (a-1) membrane glycoprotein and (a-2) envelope glycoprotein, which are marked in red in both (b) and (c), (a-3) SARS-CoV-2 spike glycoprotein (indicated by black lines labeled as "s-peaks" in both Fig. 2(b) and (c), and (a-4) lentivirus packaging vector (marked in grey in both (b) and (c)), which corresponds to the possible peaks that appear in the spectra of both analytes using (b) Au NC and (c) Au NPs/$pZrO_2$. Peaks with the corresponding Raman vibration modes and assignments in Table 1 are also marked as s and s' in (b) and (c), respectively. The difference of the genetic material inside the virus, as illustrated in (a), is not of concern in this study since SERS method is only effective to the detection of surface components of an analyte. The peak marked as (*) corresponds to an observed peak present in A.3 variant but not in S pseudovirus. (For interpretation of the references to colour in this figure legend, the reader is referred to the Web version of this article.)

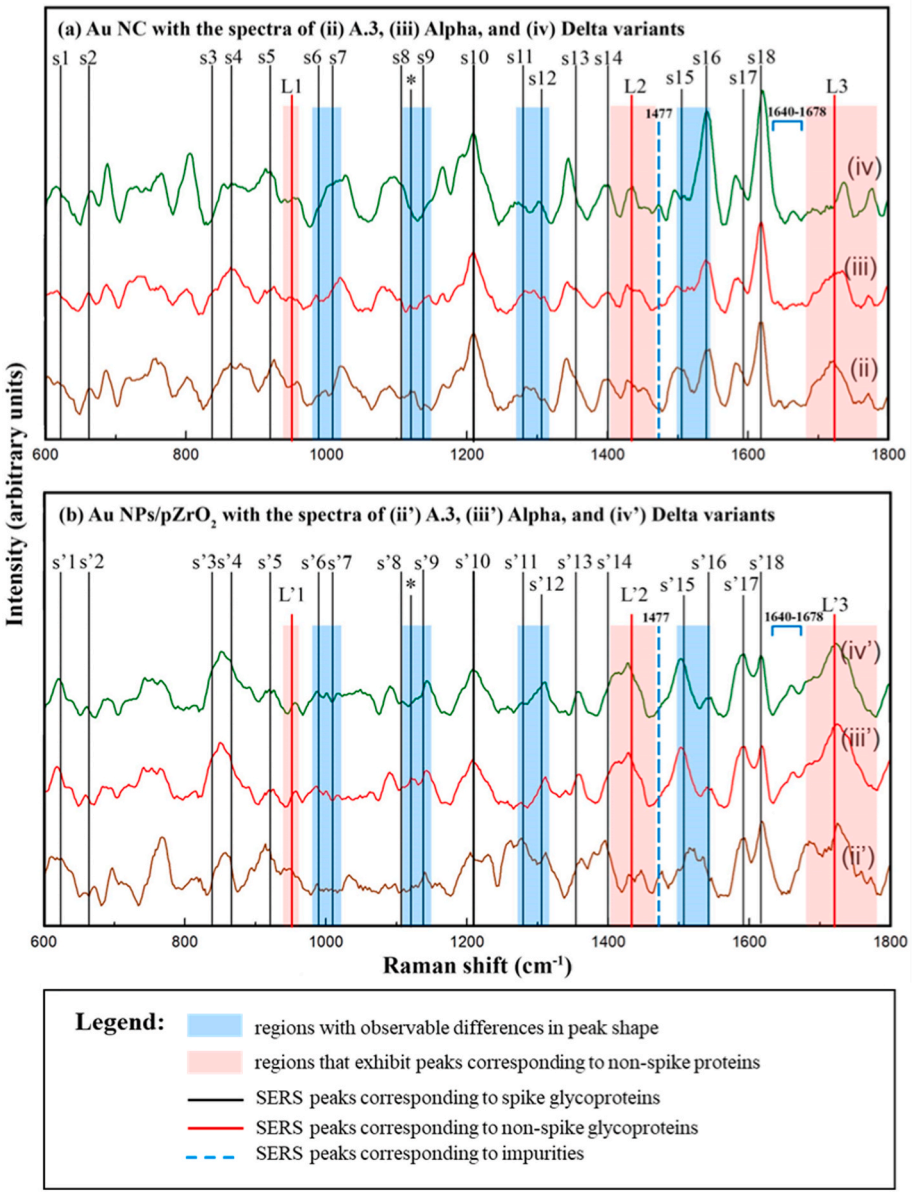

Fig. 3. SERS spectra produced from the substrates (a) Au NC and (b) Au NPs/$pZrO_2$ with SARS-CoV-2 variants: (ii)/(ii') A.3, (iii)/(iii') Alpha, and (iv)/(iv') Delta variants. Regions shaded in red correspond to membrane/envelope glycoproteins, while those shaded in blue are regions exhibiting variations in peak shapes among three variants. The peaks corresponding to spike glycoproteins are also indicated as s1/s'1 to s17/s'17 similar to Fig. 2. Moreover, the peak at 1477 cm^{-1} is marked, corresponding to impurities in the analyte sample, and the region at 1640-1678 cm^{-1} represents Amide I. (For interpretation of the references to colour in this figure legend, the reader is referred to the Web version of this article.)

peaks, labeled s1 to s18 in (i) and (ii) for Au NC and s'1 to s'18 in (i') and (ii') for Au NPs/$pZrO_2$, for any form of spike glycoproteins listed in Table 1 [21,30–32]. Spike glycoproteins (a-3 L) and (a-3 P) comprised of S1 and S2 chains are mainly exposed to the generated hotspot regions. Regions L1 to L3 in Fig. 2(b) and regions L1′ to L3′ in Fig. 2(c) are marked in red and correspond to non-spike proteins (a-1) or (a-2). Regions marked in grey for (a-4) are also identifiable on both substrates, but some signal intensities for (i') are weaker due to the substrates used.

To distinguish the two viruses, for cases of (i) and (ii), the peaks s9, s11, s15, and s17 of S pseudovirus are shown to be prominent, while the peaks s10, s14, s16, and s18 of A.3 variant are noticeable. The peak (*) for A.3 variant is significant in (ii) but less sensitive in (ii'). The regions marked in blue show differences in peak shape, most likely due to the substrate and instrumentation used. In Table 1, the spectra and assigned peaks in the literatures may differ from the quality of spike glycoproteins received, e.g., in the form of dissociated or inactivated proteins.

3.2. *Substrate-to-analyte effect for differentiating live SARS-CoV-2 variants*

Au NC and Au NPs/$pZrO_2$ were used to explore the substrate-to-analyte effect and to distinguish Alpha and Delta variants from A.3 variant. In Fig. 3(a) and (b), Au NCs and Au NPs/$pZrO_2$ were used for (ii), (iii), and (iv) and (ii'), (iii'), and (iv'), respectively. The characteristic peaks s1 to s18 and s'1 to s'18 of the spike glycoprotein (a-3 L) are labeled, and non-spike glycoproteins (a-1) or (a-2) with regions L1 to L3 and L′1 to L′3 from A.3 variant are marked in red for reference. Four regions for each substrate are marked in blue to indicate regions where differences in peak shape/intensity can be observed between/among variants. The regions s6/s7 and s'6/s'7, and s8/s9 and s'8/s'9 differ slightly among the three variants, most likely from amino acids and amide III. Since mutated sites in S1 chain of spike glycoprotein are expected to be exposed to hotspot(s), these small changes in the spectrum may be important for distinguishing variants. The region s11/s12 can be used to differentiate Delta variant from A.3 and Alpha variants; however, regions s'11/s'12 and s'15/s'16 can be used to differentiate Alpha and Delta variants from A.3 variant, most likely from amides III and II,

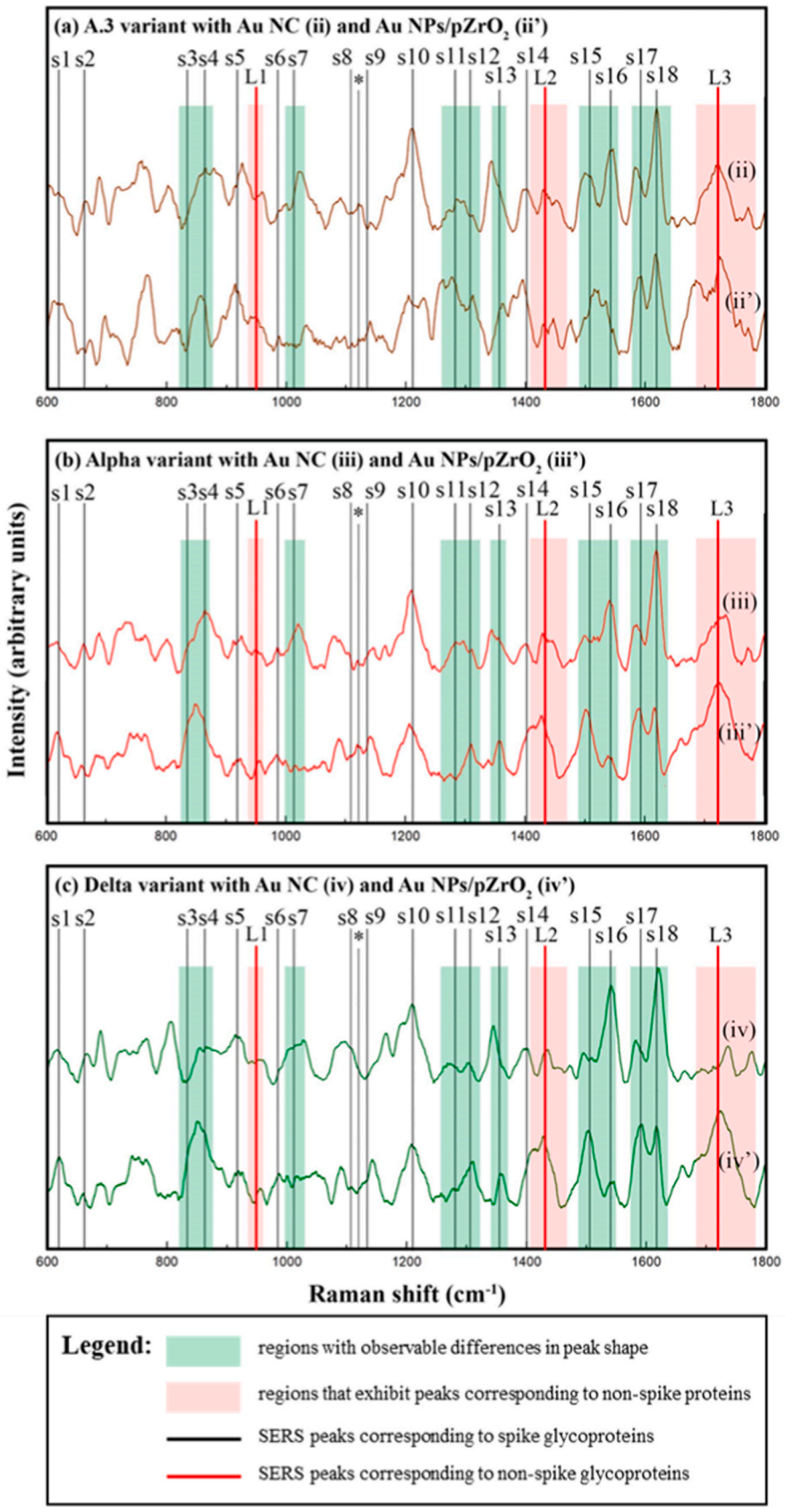

Fig. 4. SERS spectra of (a) A.3, (b) Alpha, and (c) Delta variants with respect to the uses of (i) Au NC and (ii) Au NPs/$pZrO_2$ as the substrates to explore the analyte(s)-to-substrate effect. Similar to Fig. 3, the regions in red correspond to the membrane/envelope glycoproteins, while those in green show differences in the peak shapes when comparing two different substrates with the same variant. (For interpretation of the references to colour in this figure legend, the reader is referred to the Web version of this article.)

Table 1
Assignment of SERS peaks based on SARS-CoV-2 spike glycoproteins, which are labeled correspondingly according to the substrate used: s for Au NC and s' for Au NPs/$pZrO_2$; references [32,33] utilizes isolated SARS-CoV-2 spike glycoproteins, while reference [20] does SARS-CoV-2 S pseudovirus in determining the peaks corresponding to the spike glycoproteins from live A.3 variant.

Label	Raman shift (cm^{-1})	Peak Assignment	Reference
s1/s'1	620	CH_2 rocking, Phenlyalanine	[32]
s2/s'2	660	CH_2 rocking, Phenlyalanine	[32]
s3/s'3	837	Ring breathing in Tyrosine	[20]
s4/s'4	863	CH_2 rocking, Tryptophan	[32]
s5/s'5	920	C–C stretching in amino acid; Glucose, Glycogen	[33]
s6/s'6	985	Tryptophan, Valine; CH_2 rocking, Phenlyalanine	[32,33]
s7/s'7	1008	Symmetric ring breathing mode in phenylalanine	[20]
s8/s'8	1100	ν-C–C aliphitic	[33]
*	1120	Tryptophan, phenylalanine	[33]
s9/s'9	1136	NH_3^+ rocking, Histidine	[32]
s10/s'10	1208	Tyrosine, Phenylalanine	[34]
s11/s'11	1284	CH_2 wagging, l-arginine	[32]
s12/s'12	1301	CH_2 twisting/wagging; Amide III in α-helix; Phenylalanine	[32,33]
s13/s'13	1358	Fermi resonance doublet of Tryptophan	[20]
s14/s'14	1400	Amide III in α-helix	[32]
–	1477	Impurities from analyte sample	[35]
s15/s'15	1506	C–N stretching mode in dATP	[20]
s16/s'16	1541	Amide II in anti-parallel β-sheet	[32]
s17/s'17	1592	Stretching of aromatic ring, Tryptophan, Phenylalanine	[32]
s18/s'18	1617	Amide I in anti-parallel β-sheet	[32]
–	1640–1678	Amide I	[36]

but relatively insignificant differences were found in the region s15/s16.

Compared with Fig. 2(b), the peaks s10, s14, s16, and s18 of A.3 variant are still significant for Alpha and Delta variants, as shown in Fig. 3(a), but not consistent with Fig. 3(b). Therefore, these four peaks are peak-specific for the detection of live SARS-Co-V-2 virus using Au NC as substrate. To differentiate the variants, peak shapes in the regions marked in blue can be considered. Furthermore, the doublets s17/s18 relative to s'17/s'18 are identical and their signal intensities are important to distinguish the substrates used. The peaks (*) are prominent in (ii) and (iii)/(iii'), less sensitive in (ii'), but not found in (iv)/(iv') for both substrates. In a recent report [32], the peak (*) at 1120 cm^{-1} was inferred to be an amino acid mutation in the spike glycoprotein associated with Alpha variant. Our results found that Alpha and A.3 variants had this particular peak (*). A peak at 1477 cm^{-1} can be observed on (iv) and (ii'); this incidental peak likely corresponds to impurities in the viral analyte sample, such as cellular debris from intracellular viral proliferation [33]. In addition, the region of 1640–1678 cm^{-1} corresponds to amide I in relation to the size of the amino acid sidechains; peak shapes and intensities differ for each substrate [34].

3.3. Analyte-to-substrate effect on substrates used to differentiate variants

The discriminative ability of the two substrates for the three variants was further compared. In Fig. 4(a), (b), and (c), six regions s3/s4, s7, s11/s12, s13, s15/s16, and s17/s18 (i.e., peaks s and s' are equal) marked in green are labeled and compared for each variant.

The peak (*) appears in A.3 and Alpha variants, but not in Delta variant. The doublet s17/s18 and the regions s7 and s13 for each variant differed depending on the substrate used, which may be related to the band-shifts caused by differences in hotspot(s) generated on the substrate. In addition, the detection ability of Au NPs/$pZrO_2$ shows different sensitivities to the regions s'7 and s3/s4. Comparing the spectra of each variant, most specific peaks or regions depends primarily on the substrate used. It also shows that each substrate has a different enhancement ability.

3.4. Limit of detection (LOD) and differentiation of variants

The synergistic hotspot effect between nanostructures on substrates and adjacent analytes after Raman laser induction is highly considered for virus detection and variant differentiation. The LOD depends on the change in analyte concentration, which should fall within the detection range or within a valid distance from the hotspot(s). As shown in Figs. 2–4, peaks s10, s14, and s18 for Au NC and s'10, s'15 and s'18 for Au NPs/$pZrO_2$ were prominent for all three variants with peak specificity for the detection of live SARS-Co-V-2 virus. In Fig. S1, three variants of the two substrates were analyzed at concentrations of 10^7, 10^6, 10^5, 10^4, 10^3, and 10^2 copies/mL. By indicating peaks s10, s14 or s15, and s18, both substrates demonstrated the ability to detect live variants with a LOD in the range of 10^3 to 10^5 copies/mL. Note that at least one measurement location can have a SERS spectrum if the LOD for variant detection is valid. In Fig. S2, the differences between the fixed-point and maxima within a region approaches are compared in terms of the variances in peak intensities as depicted by error bars. There are two approaches presented since given in a set of replicate spectra, the maximum points corresponding to a characteristic peak may vary due to the resolution of the portable spectrometer being less precise than that of a laboratory spectrometer. With the fixed-point approach, if a line is to be drawn on a fixed position, not all maxima from nine spectra would coincide with the line, due to the slight peak shifting as a consequence of the resolution of the portable spectrometer. Considering Fig. S2 (a) and (b) wherein the fixed-point approach was applied, variance is more apparent at higher (10^5-10^7) than at lower concentrations. Furthermore, the error bars exhibited with the fixed-point approach are much higher than when the maximum within a region approach, as shown in Fig. S2 (c) and (d), is used, wherein error bars show mostly below 3% in the measurements. With the maximum within the region approach, the peak shifts resulting from the portable spectrometer resolution are taken into consideration, minimizing the variance. With discrepancies between these approaches, averaging the nine spectra eliminates these inconsistencies, to obtain one representative spectrum that takes into consideration the slight peak shifts that were observed due to the resolution of the portable spectrometer. At higher concentrations, such as 10^3 to 10^5 copies/mL, all nine measurements could detect the target virus and obtain SERS spectra; their signal intensities for specific peaks only reached comparable (or saturated) values, which was mainly independent of the concentration used. For Au NC, even at low concentration such as 10^4 copies/mL, the measured signal intensity remains significant if detectable.

To distinguish differences between variants, peak shapes in regions s11/s12, s15/s16, and s17/s18 (s and s') can be used to distinguish variants of the substrate used. More importantly, the doublets s15/16 and s17/s18 are very identical. In addition, as previously described, regions s7 and s13 and peak (*) can be used to differentiate the substrate or variant used.

4. Discussion

Label-free and substrate-based SERS method has been applied to detect live SARS-Co-V-2 virus, enabling sensitive and rapid identification by spectroscopic analysis of characteristic peaks of its outer membrane proteins. Using a selected wavelength of Raman laser, Au NCs and Au NPs/$pZrO_2$ were cross-examined with three live SARS-Co-V-2 variants to understand the synergistic integration effect of nanostructures

and target viruses on SERS substrates. The synthetic S pseudovirus is first related to A.3 variant for reference; both two live viruses have the same spike glycoprotein with synthetic and live forms, they differ in the membrane and envelope glycoproteins of A.3 variant and the lentiviral packaging vector of S pseudovirus, as shown in Fig. 2(a).

Second, despite differences in the acquisition method and quality of the spike glycoprotein used in this study compared with other studies, the peaks assigned as spike glycoprotein in this study also matched those in the literatures. In Fig. 2(b) and (c), the assigned peaks associated with spike glycoprotein are labeled. Most importantly, the peaks s9, s11, s15, and s17 of S pseudovirus are more prominent [20], while the peaks s10, s14, s16, and s18 for A.3 variant are more pronounced. Therefore, common peaks and peaks specific to A.3 variant can be used as a reference to distinguish from Alpha and Delta variants.

Third, to take full advantage of the hotspot, the analyte should be exposed to as many hotspots as possible; since SARS-CoV-2 virus particle is a relatively large analyte, a properly designed SERS substrate is required such that its size needs to be matched to the analyte. The spike glycoprotein is a major component of the virus surface, which is essential to obtain mutation-related information, as shown in Fig. 5(a) (i-iii). The spike glycoprotein is divided into S1 and S2 chains, but mutations commonly occur in S1, which is basically the tip of the spike glycoprotein exposed to the external environment, making it the part that is more exposed to the hotspots. To differentiate the variants, the obtained spectra were cross-examined using two dissimilar substrates, which exhibited differences in the electromagnetic mechanism – Au NC forming one large hotspot and Au NPs/$pZrO_2$ producing many small hotspots, as illustrated in Fig. 5(b) (i) and (ii). Through differences in hotspot(s), they may have different substrate-analyte effects and facilitate the construction of SERS spectra of variants with common and specific peaks. Substrate-dependent effects are primarily determined by certain SERS peak shapes in specific spectral regions.

As shown in Figs. 3 and 4, peak shape changes in regions s3/s4, s7, s11/s12, s13, s15/s16, and s17/s18 (i.e., peaks s and s' are equal) can differentiate variants when a specific substrate is used. The doublets s15/s16 and s17/s18 have different peak shapes and signal intensities, regardless of the variant used. Some spectral changes may also occur, such as band shifts and disappearance of characteristic peaks, implying that the outcome resulting from the synergistic integration effect between SERS-active substrate and the spike glycoprotein is crucial. These differences may be due to differences in substrate morphology leading to different hotspot shapes and affecting their ability to enhance spectral intensity.

Fourth, the synergistic hotspot effect between nanostructures on the substrate and adjacent analytes is thus responsible for virus detection and variant differentiation. Using the same substrate, at higher analyte concentrations, the signal intensities of peaks s10, s14 or s15, and s18 were comparable and almost independent of the concentration used, while at low concentrations, their detected signal intensity is still evident. As shown in Fig. 5(c) (i), (ii) and (iii), there is a possibility of the analytes stacking upon each other, in particular at high concentrations, that results in unequal exposure of the analytes to hotspots. Furthermore, when analytes come into contact with the substrate surface, they are expected to be configured in multiple orientations, the spike

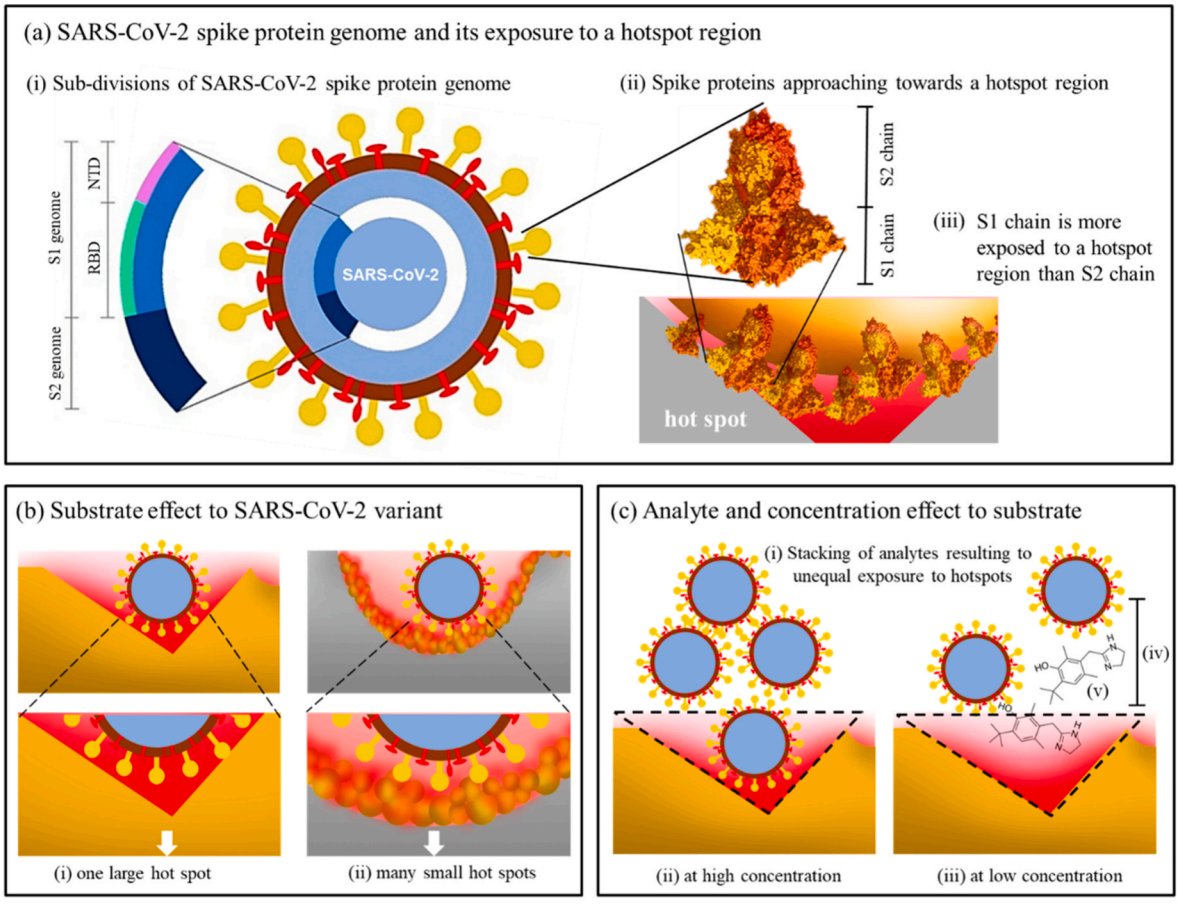

Fig. 5. The structure of SARS-CoV-2 spike glycoprotein is shown in (a), and mutations occur on the S1 genome (i). Between S1 and S2 chains (ii), S1 is more dominantly exposed to the hotspot regions (iii). SERS signal enhancement is based on (b) substrate-to-analyte and (c) analyte-to-substrate effects. In (b), Au NC (i) and Au NPs/$pZrO_2$ (ii) differ in morphologies resulting to different hotspot shapes; (c), the distribution of analytes (i) leads to unequal exposure to the hotspot(s); the concentration of analytes (ii) and (iii), the distance of the analyte from the hotspot(s) (iv), and the presence of interfering substances (v) may also influence the resulting SERS signals.

glycoproteins are not evenly spaced, and hotspot coverage may vary across all viral particles. Therefore, SERS peak intensity of each variant may vary, depending on how the virus is distributed on the substrate surface or how many viral particles can be accommodated within the nanostructured unit. For Au NC, since the region of the strongest hotspot is expected to be at the bottom of the nanocavity, SERS peaks position can remain unchanged, but their SERS intensities (or peaks shapes) are not optimized as the analytes aggregate away from the hotspot [12]. Although the concentration of analytes increases further, they tend to stack together in such a way that not all of these analytes are effectively exposed to the hotspot(s), so the synergistic effect is considered weak or undetectable. This is reflected in the results, as the intensity of the characteristic peaks is almost constant despite further increases in concentration.

At low concentrations, the reduction in intensity is mainly attributed to a reduction in the number of detectable viral particles, as shown in Fig. 5(c). However, there may be cases where viral particles are present, but the distance between the viral particles and the effective hotspot(s) may be so large that the resulting signal is too weak to be reflected as a characteristic peak, shown in (iv), e.g., the presence of other substances contained in live sample forms a considerable barrier between the analyte and the substrate, resulting in a weaker hotspot effect on the analytes. It should also be noted that at lower concentrations, it would mean less viral analytes, and these are sparsely and randomly situated throughout the substrate. This is one of the limitations of the study that should be considered for further improvement in succeeding studies. For the addition of oxymetazoline, shown in (v), a non-SERS-active interfering substance, using Au NC as substrate for the three variants, specific peaks s10, s14, and s18 remained unchanged at 10^5 copies/mL LOD (shown in SD 4), while the peak (*) decreased significantly. This means that the complicity of the synergistic hotspot effect increases with the presence of different interfering substances.

5. Conclusion

The synergistic hotspot effect between nanostructures on specially designed SERS-active substrates and adjacent analytes is responsible for SARS-Co-V-2 virus detection and variant differentiation. Their common signal intensities at peaks s10, s14 or s15 and s18 peaks were comparable and almost independent of the concentration used, while at low concentrations, the detected signal intensities remained significant. Variations in peak shape in regions s3/s4, s7, s11/s12, s13, s15/s16, and s17/s18 can further differentiate variants when using specific substrates, while the doublets s15/s16 and s17/s18 have distinct peaks shape and signal intensity, regardless of the variant used. In the presence of interfering substances at LOD levels, some unaffected peaks can still be used as important references for reliable detection. This substrate-based label-free method enables the detection of SARS-CoV-2 virus and its variants, and is of great value for more comprehensive and specific studies to distinguish upcoming variants.

CRediT authorship contribution statement

Jaya Sitjar: Conceptualization, Methodology, Data curation, Writing – original draft. **Jiunn-Der Liao:** Conceptualization, Methodology, Supervision, Validation, Writing – review & editing, Writing – original draft. **Han Lee:** Methodology, Data curation. **Huey-Pin Tsai:** Conceptualization, Methodology, Data curation. **Jen-Ren Wang:** Conceptualization, Methodology, Validation. **Chien-Hsiung Chen:** Data curation, Investigation. **Hao Wang:** Data curation, Investigation. **Bernard Haochih Liu:** Visualization.

Declaration of competing interest

The authors declare the following financial interests/personal relationships which may be considered as potential competing interests: Jiunn-Der Liao reports financial support was provided by National Science Council of Taiwan. Jiunn-Der Liao reports a relationship with National Science Council of Taiwan that includes: funding grants. Jiunn-Der Liao has patent pending to National Cheng Kung University.

Data availability

Data will be made available on request.

Acknowledgements

This work was supported by the National Science Council of Taiwan (grant numbers: NSC 110-2221-E-006 -014 -MY3, 109-2224-E-006-008, 109-2327-B-006-005, 109-2811-E-006-531-MY2, and 111-2321-B-006-009 and National Cheng Kung University Hospital (grant number: NCKUH-11108001). The BSL-3 Virology Laboratory of National Cheng Kung University Hospital, Tainan, Taiwan (with authorization), and Center for Drug Evaluation (CDE) of Taiwan (case number: 109IDX08030). The authors declare no conflict of interest.

Appendix A. Supplementary data

Supplementary data to this article can be found online at https://doi.org/10.1016/j.aca.2023.341151.

References

[1] M. Lotfi, M.R. Hamblin, N. Rezaei, COVID-19: transmission, prevention, and potential therapeutic opportunities, Clin. Chim. Acta 508 (2020) 254–266, https://doi.org/10.1016/j.cca.2020.05.044.
[2] S. Baloch, M.A. Baloch, T. Zheng, X. Pei, The coronavirus disease 2019 (COVID-19) pandemic, Tohoku J. Exp. Med. 250 (2020) 271–278, https://doi.org/10.1620/tjem.250.271.
[3] R. Chilamakuri, S. Agarwal, COVID-19: Characteristics and Therapeutics, 2021, pp. 1–29, 2012.
[4] S.S. Mithani, A.B. Bota, D.T. Zhu, K. Wilson, A scoping review of global vaccine certificate solutions for COVID-19, Hum. Vaccines Immunother. 18 (2022) 1–12, https://doi.org/10.1080/21645515.2021.1969849.
[5] D. Weissman, M. Alameh, T. De Silva, B.F. Haynes, B. Korber, D.C. Montefiori, D. Weissman, M. Alameh, T. De Silva, P. Collini, H. Hornsby, R. Brown, D614G spike mutation increases SARS CoV-2 susceptibility to neutralization ll ll short article D614G spike mutation increases SARS CoV-2 susceptibility to neutralization, Cell Host Microbe 29 (2021) 23–31, https://doi.org/10.1016/j.chom.2020.11.012.
[6] W.G. dos Santos, Impact of virus genetic variability and host immunity for the success of COVID-19 vaccines, Biomed. Pharmacother. 136 (2021), https://doi.org/10.1016/j.biopha.2021.111272.
[7] J. Chen, H. Lu, New challenges to fighting COVID-19: virus variants, potential vaccines, and development of antivirals, Biosci. Trends. 15 (2021) 126–128, https://doi.org/10.5582/bst.2021.01092.
[8] C. Stephan, Comparison of the performance of the PanBio COVID-19 antigen test in SARS-CoV-2 B.1.1.7 (Alpha) variants versus non-B.1.1.7 variants, Microbiol. Spectr. 9 (2021) 1–22.
[9] C. Reynard, J.A. Allen, B. Shinkins, G. Prestwich, J. Goves, K. Davies, R. Body, COVID-19 rapid diagnostics: practice review, Emerg. Med. J. 39 (2022) 70–76, https://doi.org/10.1136/emermed-2021-211814.
[10] O. Vandenberg, D. Martiny, O. Rochas, A. van Belkum, Z. Kozlakidis, Considerations for diagnostic COVID-19 tests, Nat. Rev. Microbiol. 19 (2021) 171–183, https://doi.org/10.1038/s41579-020-00461-z.
[11] E. Sheikhzadeh, S. Eissa, A. Ismail, M. Zourob, Diagnostic techniques for COVID-19 and new developments, Talanta (2020) 220.
[12] J. Sitjar, J. Der Liao, H. Lee, H.P. Tsai, J.R. Wang, P.Y. Liu, Challenges of SERS technology as a non-nucleic acid or -antigen detection method for SARS-CoV-2 virus and its variants, Biosens. Bioelectron. 181 (2021), 113153, https://doi.org/10.1016/j.bios.2021.113153.
[13] H.A. Hussein, R.Y.A. Hassan, M. Chino, F. Febbraio, Point-of-care diagnostics of covid-19: from current work to future perspectives, Sensors 20 (2020) 1–28, https://doi.org/10.3390/s20154289.
[14] F. Mollarasouli, N. Zare-Shehneh, M. Ghaedi, A review on corona virus disease 2019 (COVID-19): current progress, clinical features and bioanalytical diagnostic methods, Microchim. Acta 189 (2022), https://doi.org/10.1007/s00604-022-05167-y.
[15] H. Chen, S.K. Park, Y. Joung, T. Kang, M.K. Lee, J. Choo, SERS-based dual-mode DNA aptasensors for rapid classification of SARS-CoV-2 and influenza A/H1N1 infection, Sensor. Actuator. B Chem. 355 (2022), 131324, https://doi.org/10.1016/j.snb.2021.131324.
[16] J. Wang, A.J. Drelich, C.M. Hopkins, S. Mecozzi, L. Li, G. Kwon, S. Hong, Gold nanoparticles in virus detection: recent advances and potential considerations for

SARS-CoV-2 testing development, Wiley Interdiscip. Rev. Nanomedicine Nanobiotechnology. 14 (2022) 1–30, https://doi.org/10.1002/wnan.1754.
[17] J. Zhang, T. Xiao, Y. Cai, B. Chen, Structure of SARS-CoV-2 spike protein, Curr. Opin. Virol. 50 (2021) 173–182, https://doi.org/10.1016/j.coviro.2021.08.010.
[18] X. Zhang, X. Zhang, C. Luo, Z. Liu, Y. Chen, S. Dong, C. Jiang, S. Yang, F. Wang, X. Xiao, Volume-enhanced Raman scattering detection of viruses, Small 15 (2019) 1–8, https://doi.org/10.1002/smll.201805516.
[19] Y. Yang, Y. Peng, C. Lin, L. Long, J. Hu, J. He, H. Zeng, Z. Huang, Z.Y. Li, M. Tanemura, J. Shi, J.R. Lombardi, X. Luo, Human ACE2-functionalized gold "virus-trap" nanostructures for accurate capture of SARS-CoV-2 and single-virus SERS detection, Nano-Micro Lett. 13 (2021) 1–13, https://doi.org/10.1007/s40820-021-00620-8.
[20] J. Sitjar, H.Z. Xu, C.Y. Liu, J.R. Wang, J. Der Liao, H.P. Tsai, H. Lee, B.H. Liu, C. W. Chang, Synergistic surface-enhanced Raman scattering effect to distinguish live SARS-CoV-2 S pseudovirus, Anal. Chim. Acta 1193 (2022), 339406, https://doi.org/10.1016/j.aca.2021.339406.
[21] J. Zhang, T. Xiao, Y. Cai, B. Chen, Structure of SARS-CoV-2 spike protein, Curr. Opin. Virol. 50 (2021) 173–182, https://doi.org/10.1016/j.coviro.2021.08.010.
[22] A.A.T. Naqvi, K. Fatima, T. Mohammad, U. Fatima, I.K. Singh, A. Singh, S.M. Atif, G. Hariprasad, G.M. Hasan, M.I. Hassan, Insights into SARS-CoV-2 genome, structure, evolution, pathogenesis and therapies: structural genomics approach, Biochim. Biophys. Acta, Mol. Basis Dis. 1866 (2020), 165878, https://doi.org/10.1016/j.bbadis.2020.165878.
[23] L. Mousavizadeh, S. Ghasemi, Genotype and phenotype of COVID-19: their roles in pathogenesis, J. Microbiol. Immunol. Infect. (2020), https://doi.org/10.1016/j.jmii.2020.03.022, 0–4.
[24] A.L.M.K. Aufer, T.O.T. Heis, K.A.A.L. Au, J.O.L.G. Ray, Laboratory Biosafety Measures Involving SARS-CoV-2 and the Classification as a Risk Group 3 Biological Agent ALEXA, 2020.
[25] W. Bain, J.S. Lee, A.M. Watson, M.S. Stitt-Fischer, Practical guidelines for collection, manipulation and inactivation of SARS-CoV-2 and COVID-19 clinical specimens, Curr. Protoc. Cytom. 93 (2020) 1–11, https://doi.org/10.1002/cpcy.77.
[26] J. Huang, J. Wen, M. Zhou, S. Ni, W. Le, G. Chen, L. Wei, Y. Zeng, D. Qi, M. Pan, J. Xu, Yan Wu, Z. Li, Y. Feng, Z. Zhao, Z. He, B. Li, S. Zhao, B. Zhang, P. Xue, S. He, K. Fang, Y. Zhao, K. Du, On-site detection of SARS-CoV-2 antigen by deep learning-based surface-enhanced Raman spectroscopy and its biochemical foundations, Anal. Chem. (2021) 9174–9182.
[27] World Health Organization, Laboratory Biosafety Guidance Related to the Novel Coronavirus (2019-nCoV), 2020. Retrieved from: https://www.who.int/emergencies/diseases/novel-coronavirus-2019/technical-guidance-publications.
[28] V.M. Corman, O. Landt, M. Kaiser, R. Molenkamp, A. Meijer, D.K. Chu, T. Bleicker, S. Brünink, J. Schneider, M.L. Schmidt, D. Mulders, B. Haagmans, B. van der Veer, S. van den Brink, L. Wijsman, G. Goderski, J.-L. Romette, J. Ellis, M. Zambon, M. Peiris, H. Goossens, C. Reusken, M. Koopmans, C. Drosten, Detection of 2019 novel coronavirus (2019-nCoV) by real-time RT-PCR, Euro Surveill. 25 (3) (2020), https://doi.org/10.2807/1560-7917.ES.2020.25.3.2000045.
[29] R.N. Lu, X. Zhao, J. Li, P. Niu, B. Yang, H. Wu, W. Wang, H. Song, B. Huang, N. Zhu, Y. Bi, X. Ma, F. Zhan, L. Wang, T. Hu, H. Zhou, Z. Hu, W. Zhou, L. Zhao, J. Chen, Y. Meng, J. Wang, Y. Lin, J. Yuan, Z. Xie, J. Ma, W.J. Liu, D.n Wang, W. Xu, E.C. Holmes, G.F. Gao, G. Wu, W. Chen, W. Shi, W. Tan, Genomic characterisation and epidemiology of 2019 novel coronavirus: implications for virus origins and receptor binding, Lancet 395 (2020) 565–574.
[30] G. Yin, L. Li, S. Lu, Y. Yin, Y. Su, Y. Zeng, M. Luo, M. Ma, H. Zhou, L. Orlandini, D. Yao, G. Liu, J. Lang, An efficient primary screening of COVID-19 by serum Raman spectroscopy, J. Raman Spectrosc. 52 (2021) 949–958, https://doi.org/10.1002/jrs.6080.
[31] C. Carlomagno, D. Bertazioli, A. Gualerzi, S. Picciolini, P.I. Banfi, A. Lax, E. Messina, J. Navarro, L. Bianchi, A. Caronni, F. Marenco, S. Monteleone, C. Arienti, M. Bedoni, COVID-19 salivary Raman fingerprint: innovative approach for the detection of current and past SARS-CoV-2 infections, Sci. Rep. 11 (2021) 1–13, https://doi.org/10.1038/s41598-021-84565-3.
[32] K. Daoudi, K. Ramachandran, H. Alawadhi, R. Boukherroub, E. Dogheche, M.A. El Khakani, M. Gaidi, Ultra-sensitive and fast optical detection of the spike protein of the SARS-CoV-2 using AgNPs/SiNWs nanohybrid based sensors, Surface. Interfac. 27 (2021), 101454, https://doi.org/10.1016/j.surfin.2021.101454.
[33] J.E. Sanchez, S.A. Jaramillo, E. Settles, J.J. Velazquez Salazar, A. Lehr, J. Gonzalez, C. Rodríguez Aranda, H.R. Navarro-Contreras, M.O. Raniere, M. Harvey, D. M. Wagner, A. Koppisch, R. Kellar, P. Keim, M. Jose Yacaman, Detection of SARS-CoV-2 and its S and N proteins using surface enhanced Raman spectroscopy, RSC Adv. 11 (2021) 25788–25794, https://doi.org/10.1039/d1ra03481b.
[34] S.W. Huang, C.H. Tai, Y.M. Hsu, D. Cheng, S.J. Hung, K.M. Chai, Y.F. Wang, J. R. Wang, Assessing the application of a pseudovirus system for emerging SARS-CoV-2 and re-emerging avian influenza virus H5 subtypes in vaccine development, Biomed. J. 43 (2020) 375–387, https://doi.org/10.1016/j.bj.2020.06.003.
[35] D. Chalapathi, S. Padmanabhan, R. Manjithaya, C. Narayana, Surface-enhanced Raman spectroscopy as a tool for distinguishing extracellular vesicles under autophagic conditions: a marker for disease diagnostics, J. Phys. Chem. B 124 (2020) 10952–10960.
[36] K. Mochalov, P. Samokhvalov, G. Nifontova, T. Tsoi, A. Sukhanova, I. Nabiev, Surface-enhanced Raman scattering of CoV-SARS-2 viral proteins in a strong coupling regime, in: Journal of Physics: Conference Series IOP Publishing, 2021, p. 2058, 1.